

## Numerical Investigation of Rock Mechanical Characteristics in Post-peak Curve Based on Combined Finite-discrete Element Method

Peitao Li<sup>1,2</sup>, Penghai Deng<sup>1,2</sup>, Quansheng Liu<sup>1,2,\*</sup> and Ping Liu<sup>1,2</sup>

<sup>1</sup>Key Laboratory of Safety for Geotechnical and Structural Engineering of Hubei Province, School of Civil Engineering, Wuhan University, Wuhan 430072, China

<sup>2</sup>State Key Laboratory of Water Resources and Hydropower Engineering Science, Wuhan University, Wuhan 430072, China

Received 2 January 2022; Accepted 19 March 2022

### Abstract

To explore the influence of confining pressure on rock mechanical properties in post-peak curve, the combined finite-discrete element method was used and the post-peak stress and fracture characteristics of rock under different confining pressures and damage degree were analyzed. Results show that the post-peak axial stress increases linearly with the confining pressure, but the higher confining pressure will also increase the fracture number. However, the fracture number is sensitive to the damage degree. Therefore, the coordination of confining pressure and damage degree provide a possibility to control the post-peak stress and fracture number simultaneously. While a smaller damage degree at the loading time is contribute to the control of rock post-peak mechanical property. The increase of post-peak stress and decline of fracture number can be achieved by an appropriate combined loading scheme. The coordination of support strength and applying time has a good prospect for the development of combined support technology.

*Keywords:* Mechanical characteristics, Confining pressure, Damage degree, Combined loading method

### 1. Introduction

At present, the large deformation control of soft rock under high stress conditions is still a great challenge to roadway engineering [1-3]. Though many achievements have been made in the support technology of soft rock roadway, the stability of soft rock roadway cannot be achieved by high-strength support method under high in-situ stress conditions [4,5]. Aiming to enhance the bearing capacity of surrounding rock, the design principle of deep roadway support has gradually changed from passive support to active support. At the same time, the support technology also achieves great progress. The support method has changed from the single method to a combination of different methods. Therefore, the combined support technology has been widely used and studied, which can make full use of surrounding rock and support materials.

In the early stage, the combined support technology was a simple superposition. After many years of research, it has developed a variety of support methods, such as bolt-shotcrete and steel meshes support, bolt-shotcrete steel and mesh belt support, bolt-shotcrete steel meshes support, etc. However, creep is an obvious characteristic of soft rock roadway, which is not fully considered in the study of the combined support technology [6-9].

The mechanism of different support methods (shotcrete, steel arch, anchor bolt, anchor cable) to surrounding rock is equivalent to applying a confining pressure on the rock at different damage degrees. The study on the influence of confining pressure on the post-peak rock is often focused on its amplitude rather than loading time. Therefore, the influence of confining pressure and loading time should be studied, which is expected to make a basis for the combined

support technology.

### 2. State of the art

The plastic zone of surrounding rock increases gradually after roadway excavation. The support force of the steel-shotcrete will increase with the delay of support time. The delayed distance for the support installation was suggested to be within the radius of roadway [10]. The surrounding rock for TBM was analyzed under different self-compacting concrete backfilling, which showed there was an optimal time for the TBM support, which could not only reduce the deformation of surrounding rock and risk of TBM jamming but also enhance the stability of the surrounding rock [11]. Since the stability of surrounding rock is affected by the support time, the surrounding rock at different time is under different post-peak stress states. If the variation of dilation of post-peak rock is ignored, it will overestimate the tunnel convergence [12,13]. So, the variation of rock mechanical properties in post-peak curve has an important impact on the stability of the surrounding rock.

Some scholars have also studied the rock mechanical characteristics of in the post-peak curve. The confining stress would place restrictions on the extension of the wing fractures and the decline of fracture angle [14,15]. Besides the confining pressure, the loading direction also affects the rock failure type. The post-peak stress-strain curves of rock under axial-strain-controlled loading were Class I, while it was Class II when the lateral-strain-controlled loading method was applied [16]. The drop modulus was also affected by tangent modulus and secant modulus, sample sizes, Poisson's ratio and the quartz content of rocks [17,18]. The mechanical characteristics of rock under different

\*E-mail address: tmsxy\_2019@126.com

damage degree was also carried, the reflection energy and dissipation energy of sandstone under impact load increased with damage degree, while the rock strength and peak strain decreased [19,20].

The post-peak mechanical properties of rock can influence on the stability of the surrounding rock of roadway engineering. However, the current study about the rock post-peak mechanical property is usually carried by two steps. Firstly, the rock is loaded to the different damage degrees and then unload to the unstressed state. Secondly, the determined confining pressure is applied, and the rock is loaded axially until failure [21]. That is inconsistent with the actual situation of the surrounding rock, especially in the plastic zone. The surrounding rock in the plastic zone is under different damage degrees and post-peak stress states at the same time. Correspondingly, the confining pressure should be applied after the peak stress point when the rock is under different damage degrees and stress states. So, an investigation of post-peak mechanical characteristics of rock is imperative which considers the actual situation of the surrounding rock.

Due to the anisotropy and heterogeneity of rock, the loading time of confining pressure corresponding to the preset post-peak damage degree of rock cannot be easily and accurately determined under the test conditions [22]. So, numerical analysis is a suitable choice for the study of rock post-peak mechanical behavior [23]. The finite-discrete element method (FDEM) is a promising numerical analysis method, which can not only accurately analyze the post-peak mechanical properties of rock, but also the fracture evolution process of rock [24-28]. Based on FDEM, aiming at providing a theoretical basis for combined support technology, the post-peak mechanical properties of rock under the single loading and combined loading methods were carried out.

The rest of this study is organized as follows. Section 3 gives the basic theory, numerical model, and parameters of FDEM. Section 4 describes the results and discussion, and finally, the conclusions are summarized in Section 5.

### 3. Methodology

#### 3.1 Basic theory

In a two-dimension FDEM model, the modeling domain is discretized with a mesh consisting of conventional triangular elements with four-node joint elements embedded between the edges of each contacting triangular element pair (Fig. 1). The triangular element is assumed to be in an elastic strain state without fracture, and the corresponding Cauchy stress is calculated by Hooke's law. Then, the fracturing of rock is simulated by the four-nodes joint elements [27]. This method can not only inherit the advantages of continuum-based modeling techniques for the computation of internal force and corresponding elastic deformations, but also the evaluation of the failure criterion and the initiation of new fractures. As for the failure process of rock, the discrete element method (DEM) concepts, Munjiza-NBS algorithms, and potential function were adopted [29]. Therefore, the translation, rotation, and interaction behaviors of discrete elements can be explicitly simulated by the FDEM model.

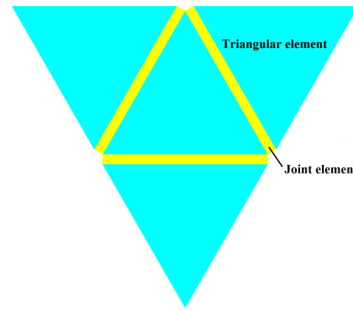
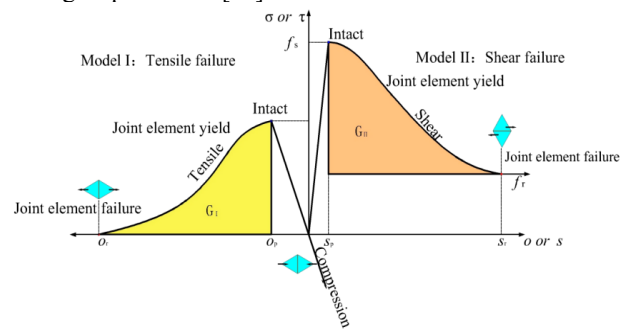
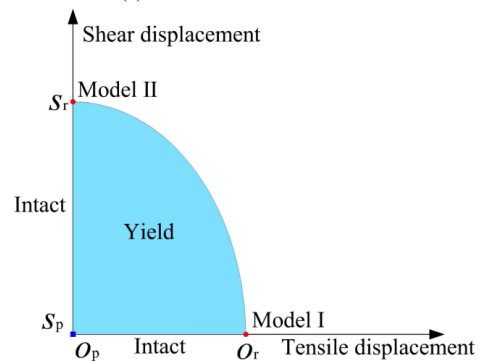


Fig. 1. FDEM modeling mesh

In the two-dimension model, the joint elements will be in yield deform and fracture under the tension mode (Model I) or shear mode (Model II) upon reaching the critical opening or sliding displacement (Fig. 2a). The fracture process based on a combination of opening and sliding displacements can be regarded as mixed Model I-II (Fig. 2b). The initiation and propagation of fracture are defined by the opening and sliding displacement [25].



(a) Tension and shear mode



(b) Mixed mode

Fig. 2. The deformation and break mode of joint element

The stress and displacement of the joint element increase with the relative displacement between two adjacent triangular elements (Fig. 3). When the joint displacement increases to a critical value, the joint element begins to yield, and the corresponding damage degree increases gradually [24]. With the increase of the joint displacement and damage degree, the joint break occurs when the joint displacement exceeds the maximum value, and the corresponding damage degree increases to 1.

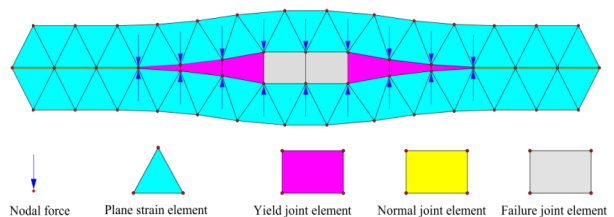


Fig. 3. The deformation and break process of joint element

As shown in Figs. 2 and 3, the damage evolution process of a joint can be divided into two parts: elastic deformation and yield deformation. During the elastic deformation stage, the joint stress is less than the joint strength, and the joint stress increases linearly with the displacement, which is defined as,

$$\begin{cases} \sigma = \frac{o}{o_p} f_t, & o < o_p \\ \tau = \frac{|s|}{s_p} f_s, & |s| < s_p \end{cases} \quad (1)$$

where,  $\sigma$  is the normal stress,  $\tau$  is the shear stress,  $o$  is the opening displacement,  $s$  is the sliding displacement,  $o_p$  is the yield opening displacement,  $s_p$  is the yield sliding displacement,  $f_t$  is the tension strength, and  $f_s$  is the shear strength. The yield deformation represents the post-peak deformation stage, which also reflects the damage evolution process [30].

During the yield deformation stage, the joint stress is determined by the damage factor and joint strength. The calculation formula is as follows:

$$\begin{cases} \sigma = f(D)f_t, & o < o_p \\ \tau = f(D)f_s, & |s| < s_p \end{cases} \quad (2)$$

where,  $f(D)$  is the softening coefficient,  $D$  is the damage factor, which is determined by the deformation of joint. So, the damage factor is defined as follows [25]:

$$D = \begin{cases} \max\left(\frac{o - o_p}{o_r - o_p}, \frac{|s| - s_p}{s_r - s_p}\right), & o > o_p \text{ or } |s| > s_p \\ \frac{o - o_p}{o_r - o_p}, & o > o_p \\ \frac{|s| - s_p}{s_r - s_p}, & |s| > s_p \\ 0, & o < o_p \text{ and } |s| < s_p \\ 1, & o > o_r \text{ or } |s| > s_r \end{cases} \quad (3)$$

where,  $o_r$  and  $s_r$  represent the ultimate displacement of opening or sliding when joint breaks, and the value is determined by  $o_r = 3l_0G_I / f_t$ ,  $s_r = 3l_0G_{II} / f_s$ , respectively.  $l_0$  represents the length of joint.  $G_I$  and  $G_{II}$  represent the breaking energy of model I and model II, respectively. The tensile strength  $f_t$  is determined by the input parameters. And the shear strength  $f_s$  obeys the Mohr-Coulomb criterion [24], which is defined as:

$$f_s = \begin{cases} c, & \sigma \geq 0 \\ c - \sigma \tan \varphi_i, & \sigma < 0 \end{cases} \quad (4)$$

where,  $c$  is cohesion strength,  $\varphi_i$  is the friction angle,  $\sigma$  is the normal stress, which is less than 0 when it is under the compression state.

The softening coefficient of material  $f(D)$  is determined by the fitting function proposed by Munjiza et al [28], the calculation formula is as follows:

$$f(D) = \left\{ 1 - \frac{a+b-1}{a+b} \exp\left[D \frac{a+bc}{(a+b)(1-a-b)}\right] \right\} [a(1-D) + b(1-D)^c] \quad (5)$$

where,  $a$ ,  $b$  and  $c$  are the fitting parameters, which are 0.63, 1.8, and 6.0, respectively.

### 3.2 Parameters of model

The rock specimens came from the No. 6 mine, located in the Pingdingshan mine, China. The physical and mechanical properties of rock specimens were tested and it is shown in Table 1. Based on the test results, the numerical model of rock with 100 mm height and 50 mm width was placed between two steel loading platens. The steel loading platen provided a highly stiff mechanical response and transmitted the velocity boundary condition directly. Based on the sensitivity study results on mesh size and loading velocity [31], the mesh size and loading velocity were 1.8 mm and 0.1 m/s, respectively.

The numerical calculation results of the uniaxial compressive strength, Young's modulus, Poisson's ratio in the FDEM model are 40.22 MPa, 13.07 GPa, and 0.21, respectively. These values are approximate to the test results. On the other hand, this study focused on the compressive behavior of rock, the stress-strain curve under compression was also well compared, as shown in Fig. 4. The proposed numerical model could reflect the mechanical properties of the specimens and was suitable for subsequent research.

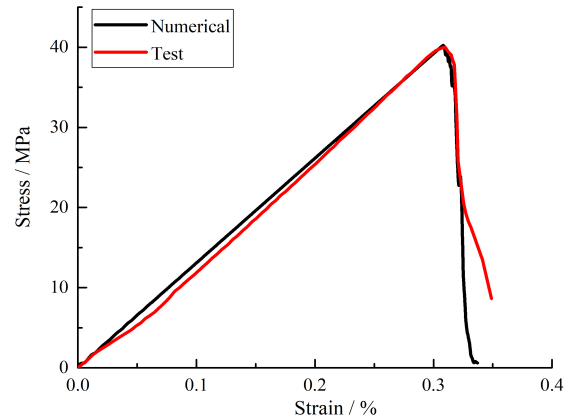


Fig. 4. Comparison of the stress-strain curve under compression

Table 1. Parameters of FDEM numerical model

Parameter	Rock	Steel plate
Model size (mm)	50×100	60×30
Element size (mm)	1.8	500
Elastic modulus (GPa)	13.2	210
Poisson's ratio	0.22	0.2
Density (kg/m <sup>3</sup> )	2600	7800
Cohesion (MPa)	13.56	7000
Tensile strength (MPa)	2.0	2000
Friction coefficient	0.58	0.5
Normal penalty of joint (GN/m)	14.6	105
Tangential penalty of joint (GN/m)	66	210
Fracture penalty parameter (GN/m)	415	210
Friction coefficient between rock and steel plate		0.1

### 3.3 Numerical analysis

To explore the post-peak mechanical behavior of rock under different damage degrees and confining pressures, the damage degree is defined as follow:

$$D_i = \frac{\sigma_c - \sigma_i}{\sigma_c - \sigma_m} \quad (6)$$

where,  $D_i$  represents the rock damage degree after the post-peak stress point.  $\sigma_c$  represents the uniaxial compressive strength.  $\sigma_i$  represents the axial stress at any time.  $\sigma_m$  is the minimum axial stress which is assumed to be 0.

The numerical investigation of rock post-peak mechanical properties under a single loading method was carried out firstly. When the post-peak axial stress decreased by 5%, 15%, 25%, 35%, 45% and 55%, the damage degree was 0.05, 0.15, 0.25, 0.35, 0.45, 0.55, respectively. Then, the corresponding axial strain ( $\varepsilon_{0.05}$ ,  $\varepsilon_{0.15}$ ,  $\varepsilon_{0.25}$ ,  $\varepsilon_{0.35}$ ,  $\varepsilon_{0.45}$ ,  $\varepsilon_{0.55}$ ) was selected as the loading reference point, and the confining pressures (1 MPa, 2 MPa, 3 MPa, 4 MPa, 5 MPa) was applied.

The combined loading method means applying different confining pressure at two loading steps corresponding to different damage degrees. For example, when the axial strain increases to  $\varepsilon_{0.05}$ , the corresponding damage degree is 0.05, and the confining pressure of 1 MPa is applied at step 1. Then, the axial strain increases to  $\varepsilon_{0.35}$ , the confining pressure of 4 MPa is applied at step 2. So, the total confining pressure of 5 MPa is applied via two steps. It can be seen from Fig. 5 that the specific process of numerical calculation is as follows.

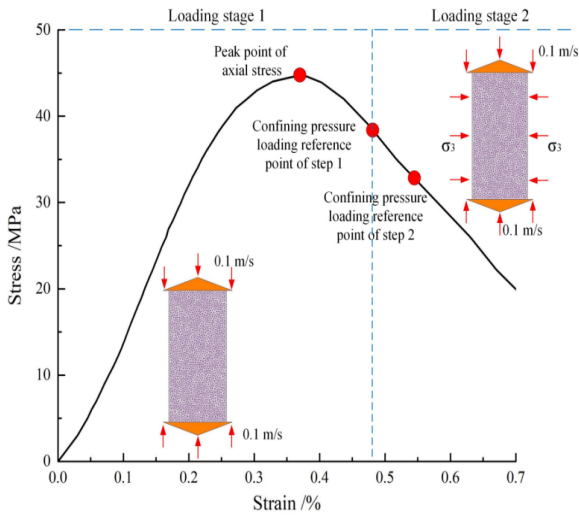


Fig. 5. The schematic diagram of numerical analysis process

- (a) Numerical model establishment and parameter calibration.
- (b) The rock was loaded by the axial displacement method. There was only axial loading during loading stage 1.
- (c) After the post-peak axial stress point, the axial strain increased to the confining pressure loading reference point of step 1, and the corresponding damage degree was  $D_i$ . Then, the preset confining pressure of step 1 was applied. Both the axial loading and confining pressure were applied during loading stage 2.

(d) With the increase of axial strain and damage degree  $D_i$ , the confining pressure of step 2 was applied, if there was a confining pressure loading reference point of step 2.

(e) The numerical analysis was suspended when the axial strain reached 1%, and the result was recorded.

(f) According to the scheme, steps (b) to (e) was repeated for other cases.

## 4. Result analysis and discussion

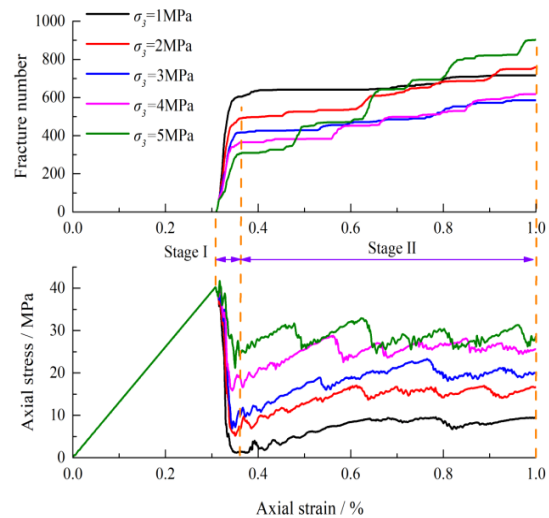
### 4.1 Single loading

#### 4.1.1 Whole deformations process

The post-peak stress determines the bearing capacity of surrounding rock and the scope of plastic zone. The minimum post-peak axial stress and maximum post-peak axial stress determine the distribution of stress field. And, the fracture number indicates the fragmentation degree of surrounding rock, which is an important index of the fracture field. So, the post-peak stress and fracture number were selected as the evaluation parameter of rock post-peak mechanical property in this study.

Firstly, the stress-strain curves and fracture number under different confining pressure (1 MPa, 2 MPa, 3 MPa, 4 MPa, 5 MPa) and damage degree (0.05, 0.15, 0.25, 0.35, 0.45, 0.55) are summarized in Fig. 6. After reaching the axial peak stress, the axial stress decreases rapidly. Then it increases after reaching the minimum residual value. Finally, the post-peak axial stress fluctuates within a certain range, which can be approximately considered to be stable. Correspondingly, the fracture number increases rapidly when the post-peak axial stress decreases. However, the growth rate of fracture number decreases rapidly when the post-peak axial stress increase from the minimum value.

It can be regarded as the dividing point when the post-peak axial stress decreases to the minimum value. Then, the post-peak deformation process can be divided into two stages (Fig. 6). During stage I, the post-peak axial stress and fracture number change rapidly, which can be called the unstable deformation stage. During stage II, the post-peak axial stress and fracture number increase slowly, which can be called the stable deformation stage.



(a)  $D_i = 0.05$

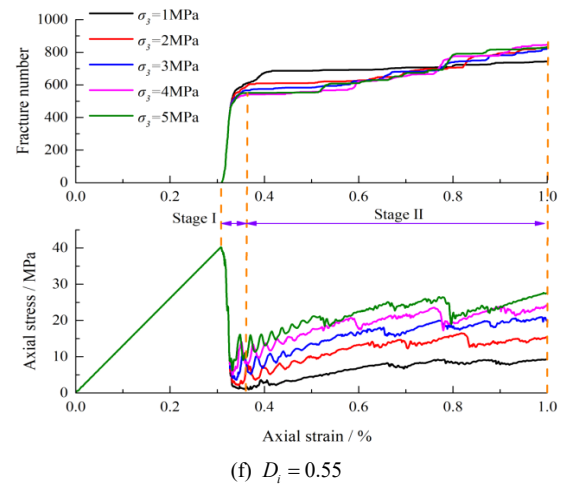
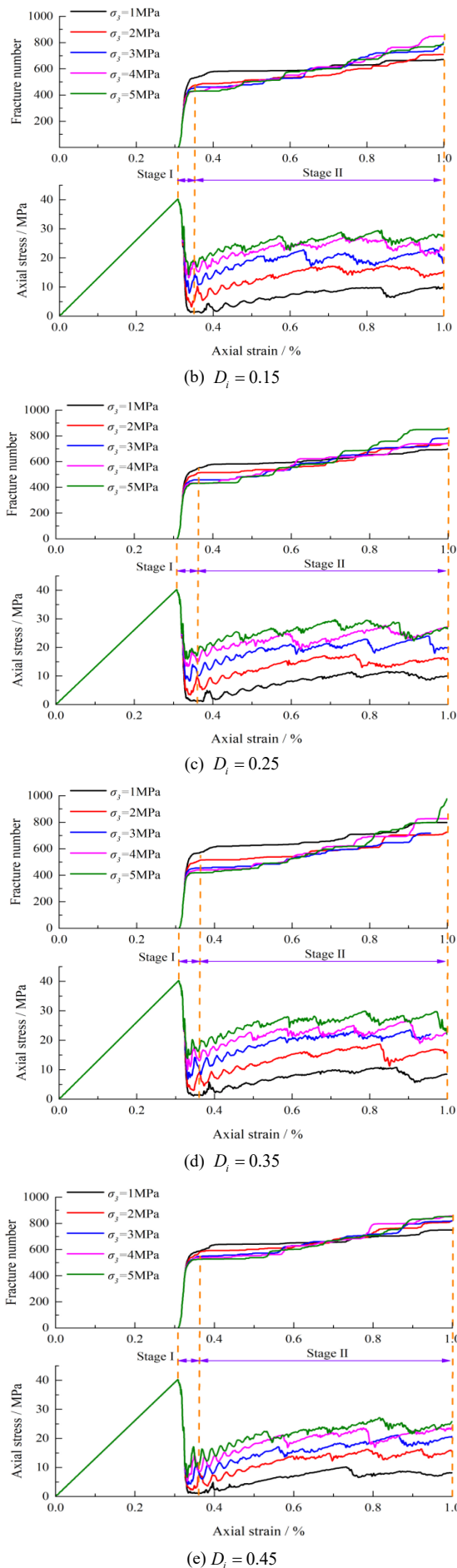


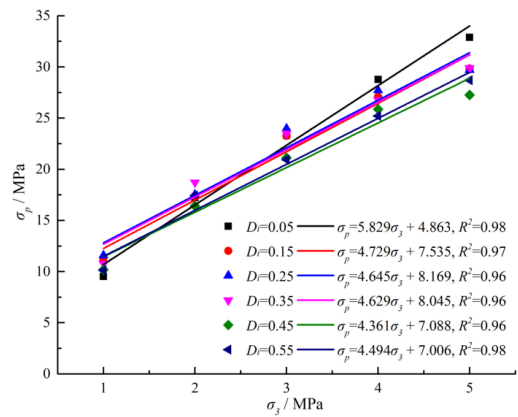
Fig. 6. The stress-strain curves and fracture number under single loading method

#### 4.1.2 Post-peak stress

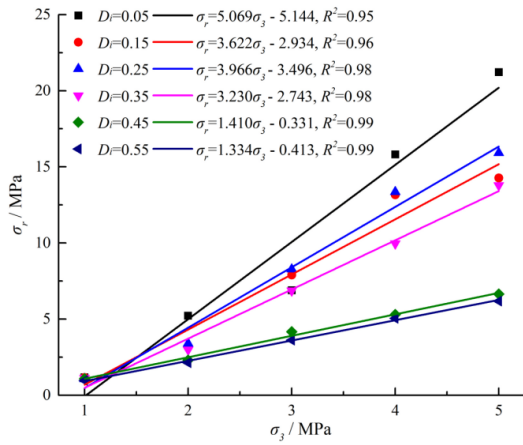
The minimum post-peak axial stress and maximum post-peak axial stress were selected as the stress evaluation index. The slope of fitting curve in the Fig. 7 shows that the smaller  $D_i$  the greater strengthen effect of confining pressure. The intercept of fitting curve is related to cohesion, which also represents the restraint of confining pressure on rock. The intercept of the fitting curve of  $\sigma_p$  increases first and then decreases with the  $D_i$ , which is consistent with the result of Zong et al [21]. The total confining pressure plays a decisive role in the amplitude of  $\sigma_p$ .

When the  $\sigma_3$  is constant, the  $\sigma_r$  decreases gradually with the increase of  $D_i$ . What is more, the decline rate of  $\sigma_r$  increases with the confining pressure. For example, if the  $D_i$  increases from 0.35 to 0.45, the reduced amplitude of  $\sigma_r$  is 3.3% when the  $\sigma_3$  is 1MPa. However, it is 51.8% when the  $\sigma_3$  is 5 MPa (Fig. 7b).

The post-peak axial stress of rock is affected by confining pressure and damage degree at the same time. When the  $D_i$  is constant,  $\sigma_r$  and  $\sigma_p$  increase linearly with  $\sigma_3$ . However, the influence of damage degree  $D_i$  is mainly reflected in the variation of  $\sigma_r$  and the  $\sigma_p$  is mainly determined by the total confining pressure.



(a) Maximum post-peak axial stress



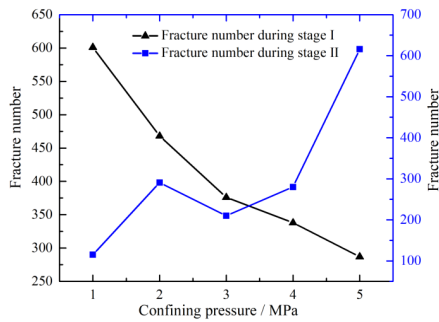
(b) Minimum post-peak axial stress

Fig. 7. The post-peak axial stress under single loading method

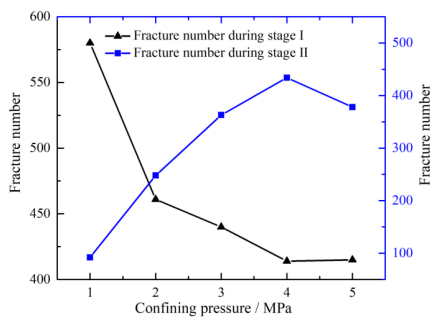
### 4.1.3 Fracture number

During stage I, the fracture number is decreased with the confining pressure. However, it is the opposite during stage II (Fig. 8). What is more, the variation of fracture number is affected by the damage degree. If the confining pressure is added from 1 MPa to 5 MPa, the fracture number during stage I is decreased by 52.2% when the  $D_i$  is 0.05, but it is 20.8% when the  $D_i$  is 0.55 (Figs. 8a, 8f). The addition of confining pressure can reduce fracture number during stage I, the corresponding decline amplitude is also increased with the decrease of  $D_i$ .

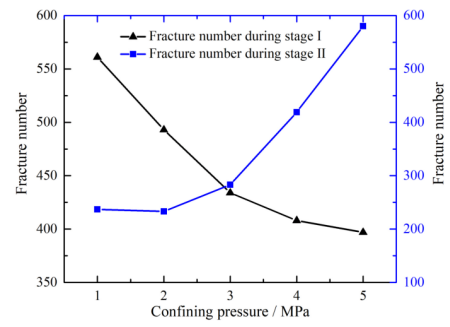
The greater confining pressure contributes to the control of rock deformation during stage I. But the accumulated strain energy is also favorable for the expansion of fracture field during stage II. When the confining pressure is added from 1MPa to 5MPa, the growth rate of fracture number during stage II decreases with the  $D_i$ . If a higher confining pressure is applied when the damage degree is small, the fracture number during stage I is reduced dramatically. It is disadvantageous for the control of fracture during stage II.



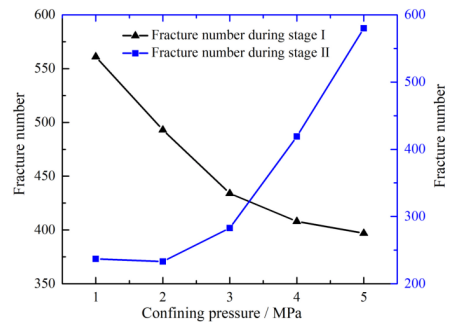
(a)  $D_i = 0.05$



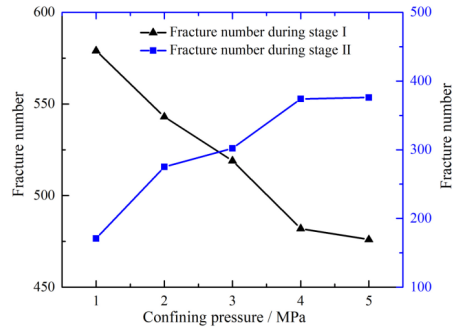
(b)  $D_i = 0.15$



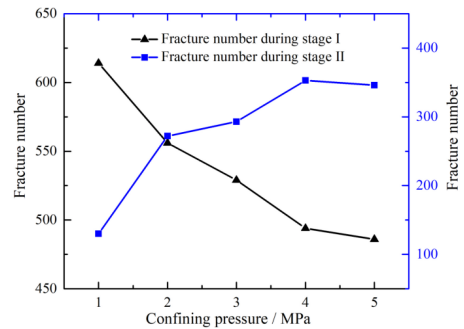
(c)  $D_i = 0.25$



(d)  $D_i = 0.35$



(e)  $D_i = 0.45$



(f)  $D_i = 0.55$

Fig. 8. The fracture number under the single loading method

If the soft surrounding rock under the high in-situ stress condition is supported with strong stiffness material, the soft rock stability of stress and deformation can be achieved during the initial stage. The accumulation of surrounding rock strain energy is apt to the initiation and expansion of fractures. Therefore, the control of fracture number must be considered, especially for stage II. To realize the increase of post-peak stress and reduction of fractures, the coordination of confining pressure and damage degree should be emphasized. The combined loading method may be applicable which can make a moderate release of strain energy and control of rock deformation and stress.

### 4.2 Combined loading

**4.2.1 Loading design and results**

If an appropriate  $\sigma_3$  is applied at step 1 when  $D_i$  is small, the increased  $\sigma_r$  and minimized fractures during stage I can be achieved at the same time. So, the  $\sigma_3$  of step 1 is assumed as 1MPa or 2 MPa, and the  $D_i$  of step 1 is 0.05 or 0.15. Then, a  $\sigma_3$  can be applied at step 2, which is aimed at

the control of  $\sigma_p$  and fracture number during stage II. Compared with the numerical result of confining pressure of 5MPa under the single loading method, the  $\sigma_3$  of step 2 is 3MPa or 4MPa and the  $D_i$  of step 2 is 0.35 and 0.45. The process of the combined loading method can refer to Fig. 5. The numerical analysis result under the combined loading method is shown in Table. 2.

**Table 2.** Numerical analysis results under the combined loading method

Group	Step 1		Step 2		Axial stress		Fracture number	
	$\sigma_3$ (MPa)	$D_i$	$\sigma_3$ (MPa)	$D_i$	$\sigma_r$ (MPa)	$\sigma_p$ (MPa)	Stage I	Stage II
H1	1	0.05	3	0.35	12.21	27.64	455	315
H2	1	0.05	4	0.35	16.07	31.77	326	398
H3	1	0.05	3	0.45	10.76	25.29	469	414
H4	1	0.05	4	0.45	14.07	27.59	463	421
H5	2	0.05	3	0.35	17.58	32.93	357	321
H6	2	0.05	4	0.35	22.39	33.62	368	416
H7	2	0.05	3	0.45	19.72	31.03	390	545
H8	2	0.05	4	0.45	23.15	34.02	291	707
H9	1	0.15	3	0.35	11.50	26.92	417	465
H10	1	0.15	4	0.35	15.05	29.54	374	481
H11	1	0.15	3	0.45	6.86	27.27	439	392
H12	1	0.15	4	0.45	8.40	29.42	430	500
H13	2	0.15	3	0.35	15.13	30.80	371	501
H14	2	0.15	4	0.35	18.68	33.88	381	435
H15	2	0.15	3	0.45	10.83	29.80	401	490
H16	2	0.15	4	0.45	12.82	30.86	398	498

**4.2.2 Effect of confining pressure**

The influence of  $\sigma_3$  in step 1 is carried (Fig. 9a). Group A1 (H1, H5) represents the comparison of groups H1 and H5. The variation of post-peak stress and fracture number when the  $\sigma_3$  of step 1 increases from 1 MPa to 2 MPa and the other condition is constant.

Under the combined loading method, both  $\sigma_p$  and  $\sigma_r$  are increased with the  $\sigma_3$  of step 1 (Fig. 9a). But the growth of  $\sigma_p$  is relatively small, which is range from 4.9% to 22.7%. The  $\sigma_r$  is affected by the  $\sigma_3$  and  $D_i$  of loading step. The fracture number during the two stages changes differently. The fracture number during stage I is mainly decreased with the  $\sigma_3$  of step 1. While it is the opposite during stage II. The post-peak axial stress and fracture number during stage II increases with the  $\sigma_3$  of step 1. But the  $\sigma_r$  is also affected by the  $D_i$  of loading step.

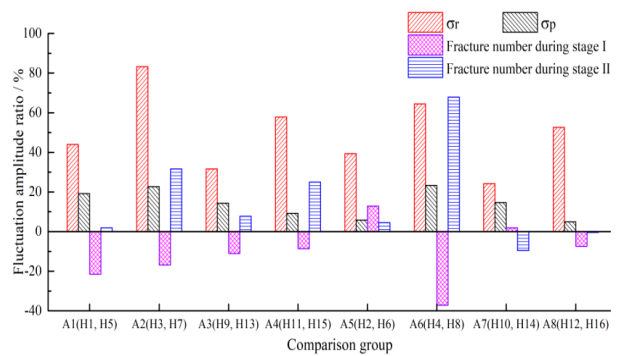
Similar to the  $\sigma_3$  of step 1, both  $\sigma_r$  and  $\sigma_p$  increase with the  $\sigma_3$  of step 2 (Fig. 9b). And, the fracture number during stage I decreases with the  $\sigma_3$  of step 2, but it increases during stage II. While the  $\sigma_r$  is affected by both the  $\sigma_3$  of step 1 and step 2. When the  $\sigma_3$  of step 1 is 1 MPa, the  $\sigma_r$  increases by 22.3-31.6% with the  $\sigma_3$  of step 2, but it decreases to 17.4-27.4% when the  $\sigma_3$  of step 1 is 2 MPa.

The increase of  $\sigma_3$  in step 1 or step 2 is a benefit for the increase of post-peak axial stress. The fracture number during stage I decreases with the increase of  $\sigma_3$ , but it will accelerate the fracture number during stage II.

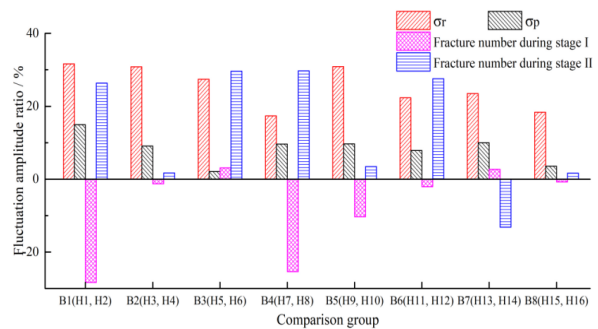
**4.2.3 Effect of damage degree**

With the increase of  $D_i$  at step 1, the  $\sigma_r$  decreases (Fig. 10a). The variation of  $\sigma_p$  is within 9.3%. Both  $\sigma_r$  and  $\sigma_p$

show a negative correlation with the  $D_i$  of step 2. While, the influence of  $D_i$  at step 1 on fracture number is complex, which is also affected by other conditions. The fracture number increases with the  $D_i$  of step 2 (Fig. 10b). The increase of  $D_i$  at step 1 or step 2 is disadvantageous for the control of post-peak stress and fracture number.



(a) The influence of  $\sigma_3$  at loading step 1



(b) The influence of  $\sigma_3$  at loading step 2

**Fig. 9.** The influence of confining pressure under the combined loading method (A1(H1, H5) represents the comparison between group H1 and H5)

However, the improvement of post-peak mechanical property of rock may be achieved by a decrease of  $D_i$  at step 2. Compared with group H12, the  $D_i$  at step 2 of group H10 is smaller and the other condition is constant. But the post-peak stress of group H10 increases and the total fracture number decreases at the same time (Fig. 10b). The increase of post-peak stress and reduction of fracture number can be achieved under the combined loading method.

When a smaller confining pressure is applied at step 1, the strain energy can be released moderately and the rock damage rate is also decreased. After an appropriate release of rock strain energy, the long-term stability of surrounding rock can be achieved when confining pressure of step 2 is applied. So, the evolution process of surrounding rock stress field and fracture field can be effectively controlled through reasonable coordination of support strength and applying time.

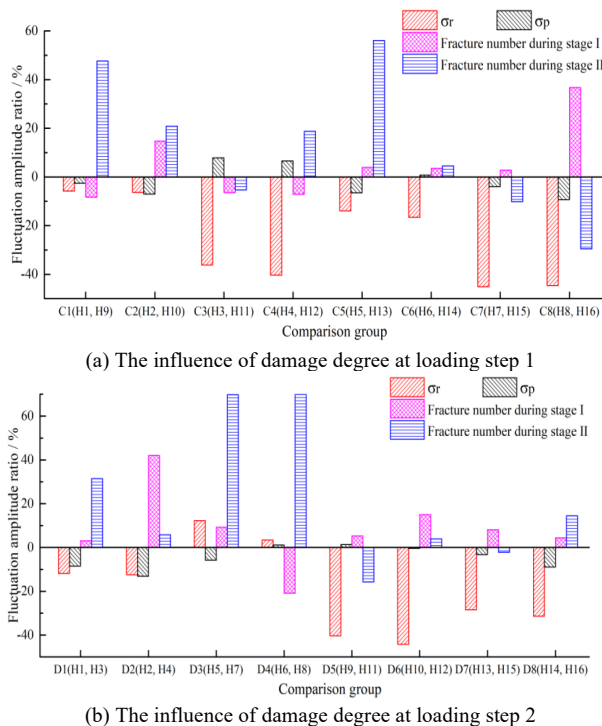


Fig. 10. The influence of damage degree under the combined loading method (C1(H1, H9) represents the comparison between group H1 and H9)

### 4.3 Discussion

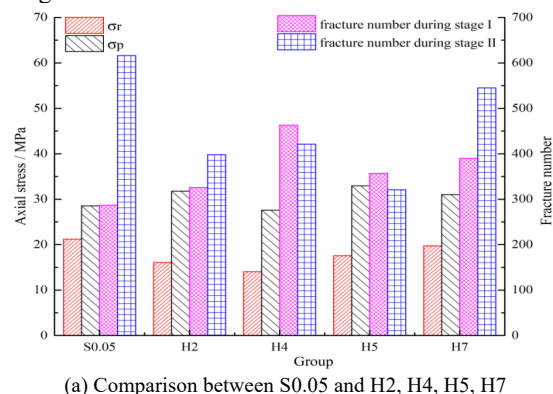
To demonstrate the significance of the coordination of loading pressure and damage degree, a comparison of the post-peak mechanical properties of rock under the single loading method and the combined loading method was carried. Under the single loading method, a confining pressure of 5 MPa is applied at different damage degrees ( $D_i = 0.05, 0.15, 0.35, 0.45$ ), which is selected as the blank group and named as S0.05, S0.15, S0.35, S0.45, respectively. The total confining pressure for the combined loading method is 5 MPa. Under the combined loading method, the  $D_i$  of step 1 is 0.05 or 0.15, and the  $D_i$  of step 2 is 0.35 or 0.45. The  $\sigma_3$  of 5MPa is applied when the  $D_i$  is 0.05 under the single loading method (group S0.05). Then, the  $D_i$  of step 1 is 0.05 under the combined loading method is regarded as the comparison group (groups H2, H4, H5, H7), as shown in Fig. 11a. The comparison with groups S0.15, S0.35, and S0.45 are shown in Figs. 11b, 11c, and 11d.

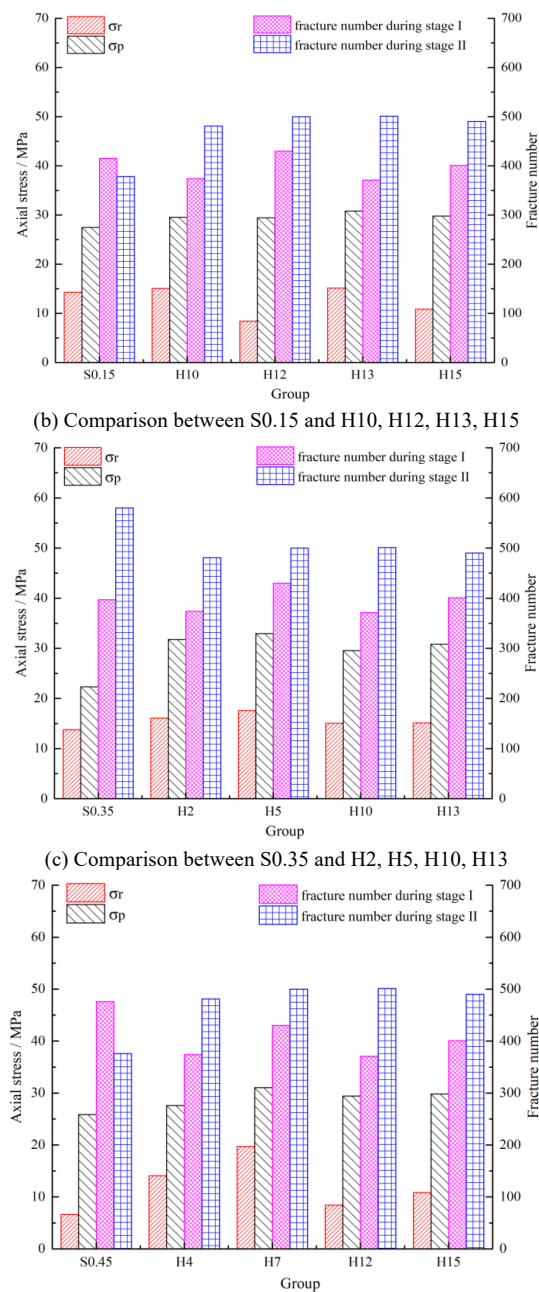
The initial confining pressure under the combined loading method is smaller than that of group S0.05. It results in a decline of  $\sigma_r$  and an increase of fracture number during stage I (Fig. 11a). The fracture number during stage II and total fracture number decrease under the combined loading method. Compared with group S0.05, the combined loading method will result in a reduction of  $\sigma_r$  and an increase of fracture number during stage I, but it is a benefit for the control of stress and fracture field during stage II.

Similar to group S0.05, both  $\sigma_p$  and total fracture numbers are larger than that of group S0.15 during stage II under the combined loading method (Fig. 11b). But the post-peak stress and fracture number are also affected by the  $D_i$  of step 2. Compared with group S0.15, when the  $D_i$  of step 2 is 0.35 (groups H10, H13), the  $\sigma_r$  increases and the fracture number during the stage I decreases, but it is opposite when the  $D_i$  of step 2 is 0.45 (groups H12, H15). In short, it is advantageous for the control of stress and fracture number under the combined loading method when the  $D_i$  of step 2 is 0.35.

When the  $\sigma_3$  of 5 MPa is applied when the  $D_i$  is 0.35 or 0.45 under the single loading method (groups S0.35, S0.45). Then, the  $D_i$  of step 2 is 0.35 or 0.45 under the combined loading method is regarded as the comparison group. The comparison with the groups S0.35 and S0.45 is similar (Figs.11c, 11d). Under the combined loading method, a smaller confining pressure is applied when the  $D_i$  of step 1 is 0.05 or 0.15. Therefore, the release rate of strain energy during the early stage is smaller than that of S0.35 and S0.45. Both  $\sigma_r$  and  $\sigma_p$  under the combined loading method are greater than that of the single loading method. What is more, the increased amplitude of  $\sigma_r$  and  $\sigma_p$  is larger when the  $D_i$  of step 1 is 0.05 (groups H2, H5). Compared with S0.35, the fracture number during stage II under the combined loading method declines. The small confining pressure applied at the early stage can not only lead to an increase of post-peak stress but also lead to a descend of fracture number.

The fracture number can be well controlled under the combined loading method than that of a higher confining pressure applied at the early stage or later stage. If higher support is applied at the early stage for once, the expansion of fracture field may occur during the later stage. Therefore, the smaller initial support should be applied timely, which can slow down the deformation of surrounding rock, and improve the residual strength of surrounding rock. Then, the secondary support also should be applied at an appropriate time. It demonstrates once the effectiveness of the combined loading method.





(d) Comparison between S0.45 and H4, H7, H12, H15

**Fig. 11.** The comparison of rock post-peak mechanical properties under the single loading method and combined loading method (S0.05 S0.15 S0.35 S0.45 represent the single loading method; H2, H4, H5, H7, H10, H12, H13, H15 represent the combined loading method and the details of loading step can refer to Tab.2)

### 5. Conclusions

To make a basis for the combined support technology and demonstrate the significance of the coordination of support strength and applying time, based on the combined finite-discrete element method, the post-peak mechanical behavior of rock was analyzed and discussed. The main conclusions are as follows:

- (1) The rock post-peak stress increases linearly with the confining pressure, but it also contributes to a greater number of fractures. The fracture number is sensitive to the damage degree when the confining pressure is applied.
- (2) The greater post-peak stress and smaller fracture number can be achieved by the reasonable coordination of confining pressure and damage degree.
- (3) The smaller confining pressure is applied at the early stage which slows down the damage rate and the release of strain energy. Both post-peak stress and fracture number under the combined loading method are improved.

Since the influence of support strength and applying time on the stability of surrounding rock does not analyze in this study. So, the deformation and stress field of surrounding rock with different support schemes will be carried in the next step, which is expected to contribute to the development of the combined support technology.

### Acknowledgements

The work work is supported by the National Natural Science Foundation of China (41941018; 51874275).

This is an Open Access article distributed under the terms of the Creative Commons Attribution License.



### References

1. Xu, X. Y., Wu, Z. J., Sun, H., Weng, L., Chu, Z., Liu, Q. S., “An extended numerical manifold method for simulation of grouting reinforcement in deep rock tunnels”. *Tunnelling and Underground Space Technology*, 115, 2021, pp. 104020.
2. Wang, S. R., Wang, Z. L., Chen, Y. B., Wang, Y. H., Huang, Q. X., “Mechanical performances analysis of tension-torsion coupling anchor cable”. *International Journal of Simulation Modelling*, 19(2), 2020, pp. 231-242.
3. Castellanza, R., Lollino, P., Ciantia, M., “A methodological approach to assess the hazard of underground cavities subjected to environmental weathering”. *Tunnelling and Underground Space Technology*, 82, 2018, pp. 278-292.
4. Zhao, Y. H., Wang, S. R., Hagan, P., Guo, W. B., “Evolution characteristics of pressure-arch and elastic energy during shallow horizontal coal mining”. *Tehnicki Vjesnik-Technical Gazette*, 25(3), 2018, pp. 867-875.
5. Wang, S. R., Wang, Y. H., Gong, J., Wang, Z. L., Huang, Q. X., Kong, F. L., “Failure mechanism and constitutive relation for an anchorage segment of an anchor cable under pull-out loading”. *Acta Mechanica*, 231(8), 2020, pp. 3305-3317.
6. Yuan, C., Wang, W. J., Huang, C., “A Study on the mechanism and controlling techniques of roadway deformations under high in situ stress conditions”. *Geotechnical and Geological Engineering*, 38(1), 2019, pp. 605-620.
7. Wang, S. R., Xiao, H. G., Zou, Z. S., Cao, C., Wang, Y. H., Wang, Z. L., “Mechanical performances of transverse rib bar during pull-out test”. *International Journal of Applied Mechanics*, 11(5), 2019, pp. 1950048.
8. Tarifard, A., Görög, P., Török, Á., “Long-term assessment of creep and water effects on tunnel lining loads in weak rocks using displacement-based direct back analysis: an example from northwest of Iran”. *Geomechanics and Geophysics for Geo-energy and Geo-resources*, 8, 2022, pp. 31.
9. Wang, S. R., Wang, Y. H., Wang, Z. L., Gong, J., Li, C. L., “Anchoring performances analysis of tension-torsion grouted anchor cable under free and non-free rotation conditions”. *DYNA*, 96(2), 2021, pp. 166-172.
10. Chen, C. H., Huang, Y., Li, G. F., “Model test and numerical simulation for support time of tunnel in loess”. *Advanced Materials Research*, 243-249, 2011, pp. 3696-3700.

11. Liu, Y. R., Hou, S. K., Li, C. Y., Zhou, H. W., Jin, F., Qin, P. X., Yang, Q., "Study on support time in double-shield TBM tunnel based on self-compacting concrete backfilling material". *Tunnelling and Underground Space Technology*, 96, 2020, pp. 103212.
12. Katebian, E., Molladavoodi, H., Practical ground response curve considering post-peak rock mass behaviour. *European Journal of Environmental and Civil Engineering*, 21(1), 2017, pp. 1090928.
13. Pérez, R. I., Alejano, L. R., Alonso, E., Arzúa, J., Araujo, M., "An assessment of the post-peak strain behavior of laboratory intact rock specimens based on different dilation models". *Procedia Engineering*, 191, 2017, pp. 394-401.
14. Zheng, Z., Feng, X. T., Yang, C. X., Zhang, X. W., Li, S. J., Qiu, S. L., "Post-peak deformation and failure behaviour of Jinping marble under true triaxial stresses". *Engineering Geology*, 265, 2020, pp. 105444.
15. Zhang, H. J., Li, C. C., "Effects of confining stress on the post-peak behaviour and fracture angle of fauske marble and iddefjord granite". *Rock Mechanics and Rock Engineering*, 52(5), 2018, pp. 1377-1385.
16. Akinbinu, V. A., "A predictive model for class II rocks post peak modulus using stochastic and backward multivariate methods". *Geotechnical and Geological Engineering*, 40(1), 2021, pp. 443-456.
17. Tutluoğlu, L., Öge, F. İ., Karpuz, C., "Relationship between pre-failure and post-failure mechanical properties of rock material of different origin". *Rock Mechanics and Rock Engineering*, 48(1), 2015, pp. 121-141.
18. Esmaeili, K., Hadjigeorgiou, J., Grenon, M., "Capturing the complete stress-strain behaviour of jointed rock using a numerical approach". *International Journal for Numerical and Analytical Methods in Geomechanics*, 39(10), 2015, pp. 1027-1044.
19. Majedi, M. R., Afrazi, M., Fakhimi, A., "A micromechanical model for simulation of rock failure under high strain rate loading". *International Journal of Civil Engineering*, 19(5), 2020, pp. 501-515.
20. Wang, Y. F., Wang, S. R., Li, Z., Jiao, H. Z., "Strength characteristics and empirical criterion of dry and saturated sandstone subjected to compression test". *Journal of Engineering Science and Technology Review*, 13(2), 2020, pp. 119-126.
21. Zong, Y. J., Han, L. J., Zhu, D., Jin, Y. H., Tian, M., "Experimental investigation on post-peak strength and deformation behavior of cracked sandstone". *Arabian Journal of Geosciences*, 13(353), 2020, pp. 1-12.
22. Munoz, H., Taheri, A., Chanda, E. K., "Pre-peak and post-peak rock strain characteristics during uniaxial compression by 3D digital image correlation". *Rock Mechanics and Rock Engineering*, 49(7), 2016, pp. 2541-2554.
23. Lollino, P., Andriani, G. F., "Role of brittle behaviour of soft calcarenites under low confinement: laboratory observations and numerical investigation". *Rock Mechanics and Rock Engineering*, 50(7), 2017, pp. 1863-1882.
24. Mahabadi, O. K., Lisjak, A., Munjiza, A., Grasselli, G., "Y-Geo: New combined finite-discrete element numerical code for geomechanical applications". *International Journal of Geomechanics*, 12(6), 2012, pp. 676-688.
25. Tatone, B. S. A., Grasselli, G., "A calibration procedure for two-dimensional laboratory-scale hybrid finite-discrete element simulations". *International Journal of Rock Mechanics and Mining Sciences*, 75, 2015, pp. 56-72.
26. Ahmadi, M., Seyedin, S. H., Seyedin, S. V., "Investigation of the mechanical performance of fiber-modified ceramic composites using finite element method". *Technical Journal*, 13(3), 2019, pp. 173-179.
27. Lisjak, A., Grasselli, G., "A review of discrete modeling techniques for fracturing processes in discontinuous rock masses". *Journal of Rock Mechanics and Geotechnical Engineering*, 6(4), 2014, pp. 301-314.
28. Munjiza, A., Bangash, T., John, N. W. M., "The combined finite-discrete element method for structural failure and collapse". *Engineering Fracture Mechanics*, 71, 2004, pp. 469-483.
29. Munjiza, A., Andrews, K., White, J., "Combined single and smeared crack model in combined finite-discrete element analysis". *International Journal for Numerical Method in Engineering*, 44, 1999, pp. 41-57.
30. Lisjak, A., Liu, Q., Zhao, Q., Mahabadi, O. K., Grasselli, G., "Numerical simulation of acoustic emission in brittle rocks by two-dimensional finite-discrete element analysis". *Geophysical Journal International*, 195(1), 2013, pp. 423-443.
31. Deng, P. H., Liu, Q. S., Ma, H., He, F., Liu, Q., "Time-dependent crack development processes around underground excavations". *Tunnelling and Underground Space Technology*, 103, 2020, pp. 103518.